Targeting cell membrane lipid rafts by stoichiometric functionalization of gold nanoparticles with a sphingolipid-binding domain peptide

David Paramelle, Daniel Nieves, Benjamin Brun, Rachel S. Kraut, and David G. Fernig*

Dr. D. Paramelle, B. Brun
Institute of Materials Research and Engineering
A*STAR (Agency for Science, Technology and Research)
3 Research Link, 117602, Singapore
E-mail: paramelled@imre.a-star.edu.sg
Dr. D. Nieves, Prof. D. G. Fernig
Department of Biochemistry, Institute of Integrative Biology
University of Liverpool, Liverpool L69 7ZB (UK)
Dr. R. S. Kraut
School of Biological Sciences
Nanyang Technological University
50 Nanyang Ave, 639798, Singapore.

A non-membrane protein-based nanoparticle agent for the tracking of lipid rafts on live cells is produced by stoichiometric functionalization of gold nanoparticles with a previously characterized sphingolipid- and cell membrane microdomain-binding domain peptide (SBD). The SBD peptide is inserted in a self-assembled monolayer of peptidol and alkane thiol ethylene glycol, on gold nanoparticles surface. The stoichiometric functionalization of nanoparticles with the SBD peptide, essential for single molecule tracking, is achieved by means of non-affinity nanoparticle purification. The SBD-nanoparticles have remarkable long-term resistance to electrolyte-induced aggregation and ligand-exchange and have no detectable non-specific binding to live cells. Binding and diffusion of SBD-nanoparticles bound to the membrane of live cells is measured by real-time photothermal microscopy and shows the dynamics of sphingolipid-enriched microdomains on cells membrane, with evidence for clustering, splitting and diffusion over time of the SBD-nanoparticle labeled membrane domains. The monofunctionalized SBD-nanoparticle is a promising targeting agent

for the tracking of lipid rafts independently of their protein composition and the labelling requires no prior modification of the cells. This approach has potential for further functionalization of the particles to manipulate the organization of, or targeting to microdomains that control signaling events and thereby lead to novel diagnostics and therapeutics.

1. Introduction

Lipid rafts are microdomains in the cell membrane with great potential as targets, because of their pivotal impact in essential cellular functions. Composed of mixtures of sphingolipids, cholesterol and membrane proteins, lipid rafts are dynamic structures with sizes ranging from nano- to few micrometers. Since their discovery in 1997,[1] lipid rafts have been investigated with the aim of understanding their biological functions and their role in pathologies as diverse as cancer and HIV infection. Initially, merely defined from their insolubility property in non-ionic detergent, major improvements have been made in the characterization of lipid rafts due to the development of techniques in microscopy, lipidomics and proteomics.[2,3] Today, it is clear that lipid rafts serve as mobile platforms on cell membranes to bring together and assemble functional supramolecular architectures, e.g., protein receptors, to activate essential cellular functions such as signal transduction and cell internalization of external materials.[4] Moreover, lipid rafts have been recently directly implicated in diseases such as the autoimmune skin blistering disease pemphigus vulgaris[5] and Alzheimer's disease.[6] Hence, new tools and the targeting of lipid rafts are essential to improve our knowledge of their function and to lead to the development of diagnostics and therapeutics aimed at lipid raft functions.

The targeting of lipid rafts is achieved with biochemical markers that recognize a sub-component of lipid microdomains present on cells membrane. To date, major efforts have been made to target membrane proteins. Glycosylphosphatidylinositol (GPI)-anchored

proteins and transmembrane proteins have been used to study the formation and dynamics of lipid microdomains by microscopy. Recently, membrane raft association of transmembrane proteins has been directly linked to the length of their transmembrane domains and palmitoylation.[7] The first methods developed for tracking membrane proteins involved in lipid rafts used specific antibodies labelled with fluorescent dyes[5] or loaded on fluorescent latex beads.[8] These methods enabled the direct observation of protein partitioning into membrane microdomains. Another approach used biotinylated peptide-coated quantum dots to track GPI-anchored avidin associated with glycosphingolipid-rich microdomains.[9] Similarly, the visualization of the nanoscale distribution and spatial relationship between T-cell receptor (TCR)/CD3 and co-receptors CD4 or CD8 during the T-cell activation has been achieved with near-field scanning optical microscopy and quantum dots coated with corresponding antibodies specific to the receptors targeted.[10]

Since the definition of lipid rafts is through lipids, an approach different from one that is membrane protein-based for lipid rafts targeting is to use a biomarker that recognizes lipid mixtures that are typical to lipid rafts. Therefore, a non-membrane protein-based lipid raft targeting approach is independent of the protein content of lipid rafts present on the cell's membrane and so in principle is universal and applicable to all cells with lipid rafts of the appropriate composition. The importance of targeting lipids in rafts, rather than proteins, is underscored by the recent demonstration that alterations of the lipid composition of rafts might be an indicator of early stages of Alzheimer's disease[11] and some cancers.[12] Hence, a targeting agent for lipids that contributes to such lipid rafts has significant potential for the development of diagnostics for such diseases.

The number of existing methods for non-membrane protein-based lipid raft targeting is currently limited. Chang et al. used a biotinylated cholera toxin B subunit to label specifically the raft constituent ganglioside GM1. Subsequently, the cells were promptly tagged with streptavidin conjugated quantum dots to avoid internalization of the biotinylated GM1 and

allow confocal microscopy imaging of the lipid rafts.[13] Other pore-forming toxins, e.g., ostreolysin A,[14] have been recently reviewed for their potential as lipid raft targeting agent.[15] Synthetic lipids functionalized with an affinity group, the tris-nitriloacetic acid (tris-NTA), were also used to measure the sorting of membrane proteins into lipid ordered and disordered lipid phases.[16] Tris-NTA lipids integrated into synthetic membranes and live cells were fluorescently tagged with poly-histidine conjugated proteins for single-molecule imaging.

The above represents substantial progress in developing non-membrane protein-based lipid rafts targeting methods. Yet, it would be advantageous to use a molecular probe that can bind specific lipids and be directly observed in real-time without additional chemical steps or modification of the cell membrane. The sphingolipid-binding domain (SBD) peptide is a 25-peptide sequence of the Alzheimer β-amyloid (Aβ) peptide[17] that binds specifically sphingolipid-enriched domains on cell membranes.[18] Fluorescently-labeled SBD peptides have been used to track sphingolipid-enriched domains and were shown to interact preferentially with raft-like lipid mixtures containing sphingomyelin, cholesterol and gangliosides.[19] Recently, the SBD probe offered new insights about lipid raft dynamics and their dependence on raft molecular composition.[20,21]

In this study, we present the preparation of stoichiometrically functionalized SBD-gold nanoparticles (SBD-nanoparticles) for the tracking of lipid rafts on live cells. We designed the SBD peptide probe for its integration in a peptidol/alkane thiol ethylene glycol self-assembled monolayer (Mix-matrix), used to passivate the surface of 8.2 nm diameter gold nanoparticles. We stoichiometrically functionalized Mix-matrix capped gold nanoparticles with the SBD peptide, essential for single molecule tracking, by a non-affinity based method using ion-exchange chromatography. Finally, we validated the specific targeting of the monofunctionalized SBD-nanoparticles to lipid rafts and observed their dynamics on live human SK-N-AS neuroblastoma cells by real-time photothermal microscopy.

2. RESULTS AND DISCUSSION

2.1. Sphingolipid-binding domain peptide ligand design for the functionalization of Mix-matrix capped gold nanoparticles

Mixtures of various short thiolated peptidols and alkane thiol ethylene glycols form highly stable self-assembled monolayers on the surface of noble metal (gold and silver) nanoparticles.[22–24] This approach prevents major biologically-related aggregation, e.g., electrolyte-induced aggregation, non-specific binding, ligand exchange, and ensures a high biocompatibility,[22–25] while preserving[24] the ease of controlled functionalization found with the less stable peptide ligand shells.[25,26] In this study, we used a mixture, so-called Mix-matrix, of the peptidol, H-CVVVT-ol, and a thiolated alkane ethylene glycol ligand, HS-C_{11}-EG_4, to form a ligand shell for the passivation of 8.2 nm diameter spherical gold nanoparticles **(Figure S1)**. We modified the 25-amino acid Aβ-derived SBD peptide in order to facilitate its insertion into the Mix-matrix ligand shell **(Figure 1)**. We added a short peptide sequence at the N-terminus, H-CVVVT, corresponding to the peptidol present in the Mix-matrix shell to ensure its incorporation into the self-assembled monolayer. In addition, we inserted a short tetra-ethylene glycol spacer between the SBD and the H-CVVVT sequence, to increase the likelihood of the SBD sequence being fully exposed on the surface of the nanoparticles. Recently, variations in the fluorescent SBD probe have been investigated to determine possible influences of the linker and the overall peptide charge on SBD binding and diffusion characteristics.[26] The study showed that a change at position 16 in the 25-amino acid SBD peptide from the most common naturally occurring residue in the wild type Aβ sequence of K to E, while lowering the pKa, suppressed aggregation, and additionally nuanced its diffusion behavior on the cell membrane, making diffusion more homogeneous, i.e., less complex. This change in behavior, however, did not in general correlate with the charge of the peptide SBD which was modified by either the addition of a C-terminal amide, or the K to E mutation. Importantly, a nuclear magnetic resonance study also demonstrated that the substitution of E

for K at position 16 does not impair the structure of the Aβ peptide.[27] Moreover, the EG$_4$-K16-COOH SBD peptide described in the aforementioned study, which contained the wild type sequence and is most analogous in construction to the nanoparticle-linked SBD peptide used here, displayed similar characteristic confined diffusion behavior typical of SBD and other microdomain probes.[18,26,28–30] In fluorescence correlation spectroscopy experiments, it also showed approximately the same fraction of probe bound to the cell membrane,[26] and the same sensitivity of the slowly-diffusing population to the raft-disrupting agent MβCD as the EG$_4$-E16-COOH and the AEEAc-E16-COOH peptides. Together, these observations indicate that the K16-containing (wild type, Aβ-identical) 25aa sequence of SBD, while it is likely to be more aggregation-prone, behaves similarly as a slowly-diffusing lipid domain marker.

2.2. Ion-exchange chromatography-based method for purification of stoichiometrically functionalized Mix-matrix capped gold nanoparticles with a charged peptide

The stoichiometric functionalization of nanoparticles generally involves a purification step to separate functionalized nanoparticles from non-functionalized nanoparticles. Previously, we took advantage of specific affinity, often, but not always from biomolecules, e.g., tris-NTA/oligo-histidine and FGF-heparin biological affinity.[23,24,31,32] However, a desired biofunctionalization may not impart such properties or they may not be easily exploited. This is the case with the SBD peptide, where its affinity for sphingolipids cannot be used for the purification by chromatography. However, the functionalization may impart a change in physicochemical properties of the nanoparticles. In the case of SBD peptide, we took advantage of its multiple charged residues to develop a novel method to stoichiometrically functionalize Mix-matrix capped gold nanoparticles with the SBD peptide based on ion-exchange chromatography.

The method is a straightforward two-step protocol **(Figure 2)** including a) the surface coating of gold nanoparticles with the Mix-matrix peptide ligands, i.e., H-CVVVT-ol and HS-C$_{11}$-EG$_4$, and the designed SBD peptide probe, H-CVVVT-EG$_4$-SBD, and b) the separation and

purification of monofunctional SBD-nanoparticles by ion-exchange chromatography. The SBD-nanoparticles may be then directly used *in vitro* for the tracking of lipid rafts on live cells (Figure 2, c). Interestingly, this non-affinity based method presents the advantages to be potentially applicable for other charged biomolecules, e.g., peptides, proteins, DNA, oligo/polysaccharides and it provides a strong link between the biomarker and the nanoparticle, i.e., a covalent bond, not present, for example in the tris-NTA/oligo-histidine conjugation approaches.[24,32] Moreover, this method enables both the purification of functionalized charged-biomolecules nanoparticles by removing the functionalized nanoparticles from the non-functionalized and the specific preparation of monofunctionalized nanoparticles.

Stoichiometrically functionalized gold nanoparticles with the H-CVVVT-EG$_4$-SBD peptide were prepared by coating citrate gold nanoparticles of 8.2 nm diameter (Figure S1) with a mixture of H-CVVVT-ol peptidol and HS-C$_{11}$-EG$_4$ ligands at a molar ratio of 70:30 and an additional molar percentage (in place of peptidol) of H-CVVVT-EG$_4$-SBD peptide ligand. The SBD ligand was added at a range of mole percentages (from 0 % to 5 %). After coating, the excess ligands were removed by centrifugation and size-exclusion chromatography (Figure 2, a). In a second stage (Figure 2, b), we used ion-exchange chromatography to isolate gold nanoparticles functionalized with charged SBD peptide ligands. The H-CVVVT-EG$_4$-SBD peptide is negatively charged in 20 mM TRIS buffer at pH 8, because of the acidic side chains of the glutamate and aspartate residues, and the C-terminal carboxylic acid more than balancing the basic side chains of the arginine and lysine residues (Figure 1A). The charge of the N-terminus amine of the cysteine is not included, because it is adjacent to the gold surface, thus it is not exposed to the solvent, as demonstrated previously by the tight packing of the Mix-matrix self-assembled monolayer and the absence of charge on Mix-matrix nanoparticles.[24] Therefore, the H-CVVVT-EG$_4$-SBD peptide will have a net negative charge, and for monofunctionalized nanoparticle (one SBD peptide per nanoparticle) this is likely to

be -5 at pH 8 (Figure 1). Each preparation of Mix-matrix capped gold nanoparticles with a different range of molar ratio of SBD peptide was purified by ion-exchange chromatography with the positively charged diethylaminoethyl (DEAE) Sepharose resin in 20 mM TRIS buffer at pH 8. After application of the nanoparticles onto the DEAE column (Figure 2, b-1), the non-functionalized nanoparticles were collected in the flow-through fraction, because their neutral charge precludes them binding,[24] whereas the negatively charged SBD-nanoparticles remained bound to the resin at the top of the column (Figure 2, b-2). SBD-functionalized nanoparticles were then eluted from the resin and collected with 1 M NaCl in 20 mM TRIS at pH 8.0 (Figure 2, b-3-4).

The percentage of SBD-nanoparticles immobilized on the DEAE resin, directly linked to the percentage of functionalized gold nanoparticles for each preparation,[24,31] was determined by comparing the UV-absorbance of the initial mixture of nanoparticles and of the functionalized nanoparticles released with the salt solution. A complete range of SBD-nanoparticles provided a titration curve **(Figure 3)**. Statistically, a population of stoichiometrically functionalized nanoparticles (with no more than 0.48% of that population possessing more than one functional ligand) can be prepared when 10 % of the total population of initial nanoparticles is functionalized.[24,31] Monofunctionalized SBD-nanoparticles were prepared by using 0.5 % of H-CVVVT-EG$_4$-SBD peptide ligand during the coating and purified by ion-exchange chromatography.

2.3. Long-term stability of SBD monofunctionalized Mix-matrix capped gold nanoparticles

The coating of small gold nanoparticles with the Mix-matrix ligand shell, i.e., H-CVVVT-ol:HS-C$_{11}$-EG$_4$ (70:30, mole/mole), provides high stability in biological media.[22,24,32] We used a previously described normalized aggregation parameter[22] based on UV-visible spectrometry to evaluate the colloidal stability of the SBD-nanoparticles overtime against electrolyte-induced aggregation and ligand-exchange reaction with a small thiolated molecule,

dithiothreitol. SBD-nanoparticles were highly stable against electrolyte-induced aggregation in 1 M NaCl at room temperature for over a day, even with a relatively high percentage of SBD peptide ligand (1%, **Figure S2**). Monofunctionalized SBD-nanoparticles were also stable in 15 mM DTT in 0.5 M NaCl at room temperature for more than a day **(Figure 4)**. Importantly, the high stability of the SBD-nanoparticles ensures their longevity for functional raft-tracking even over extended imaging times.

2.4. Lipid raft tracking with SBD monofunctionalized Mix-matrix capped gold nanoparticles by photothermal imaging

The efficiency of the monofunctionalized SBD-nanoparticles to target lipid rafts was evaluated with live human SK-N-AS neuroblastoma cells. We used a homebuilt photothermal microscope[33,34] to visualize the SBD-nanoparticles on the cell membrane. After incubation of a solution of 125 nM of SBD-nanoparticles with the SK-N-AS cells, unbound nanoparticles were washed off before imaging. It was very clear from control experiments that non-functionalized Mix-matrix capped gold nanoparticles did not have any detectable non-specific binding with the cells, with the photothermal signal detected only coming from mitochondria under photothermal excitation **(Figure 5A)**, as seen previously with these nanoparticles.[32] On the other hand, multiple bright dots were observed when SBD-nanoparticles were incubated with the cells, associated with the cell membrane (Figure 5B, white arrows). The photothermal peaks observed are significantly higher than the observed background from the mitochondrial signal from which they are easily distinguished (Figure 5C). The binding of SBD-nanoparticles to the SK-N-AS cells was observed at a lower concentration (125 nM) than previously described (5 μM) with a fluorescent tagged SBD, reflecting the differences in sensitivity of detection of the nanoparticle *versus* the fluorophore probes.[19] The analysis of the intensity of individual photothermal peaks on the cells, compared to that of individual nanoparticles, showed that the former were due to clusters of gold nanoparticles **(Figure S3-S5 and Table S1-S3)**. By dividing the intensity of the photothermal peaks within the image

by the intensity of a single 8.2 nm gold nanoparticle in this system, it was possible to estimate the number of SBD-nanoparticles present. The analysis of the photothermal signal intensity indicated the presence of multiple SBD-nanoparticles within a diffraction-limited area (ranging from 3 nanoparticles up to a peak value in one instance of 270 nanoparticles; Tables S1-S3). These may arise through multiple SBD-nanoparticles binding one raft or to multiple lipid rafts. It should be noted that the analysis is likely to give an over representation of domains with higher numbers of SBD-nanoparticles, as the thresholding used here will eliminate peaks whose intensity is very similar to the peak of mitochondrial signals measured in unlabeled cells, for example, peaks arising from one or few SBD-nanoparticles. In some instances the mitochondrial signal present around the nucleus may have a contributory effect to the measured nanoparticle number (peaks marked with an asterisk in Tables S1-S3). Interestingly, we observed diffusion of SBD-nanoparticles within the cell membrane. For instance, imaging of the same cells over time, i.e., approximately 10 min between images, showed obvious movement of multiple nanoparticle clusters, and the appearance of new peaks within the same area (Figure 5C and 5D). The movement of putative single SBD-nanoparticles was also observed, owing to the appearance of "streaks" within the image, and correspond to the movement of single nanoparticle labeled lipid rafts parallel to the scan direction.[32] The distances observed of clusters travelled when consecutive images were taken with 10 min intervals ranged from 1 μm up to more than 10 μm (Figure 5C-5F). During the imaging, some movement of SK-N-AS cells on the dish was observed and so this will be contributing, in part, to some of the SBD-nanoparticles movement between images.

The SBD peptide recognizes uniquely lipids such as the sphingolipids sphingomyelin and gangliosides that are thought to potentially cluster into domains or lipid rafts,[19,26] and the nanoparticles are monofunctionalized with SBD peptide. Therefore, the cell membrane association observed with clusters of SBD-nanoparticles, but not with the control non-functionalized nanoparticles, presumably reflects the interaction of the SBD peptide with its

lipid targets in lipid rafts. Moreover, the observed movement of the SBD-nanoparticles within one image indicates that the lipid rafts are dynamic. Movement observed between images will also reflect the dynamics of lipid rafts, though other factors may contribute on these longer timescales, such as cell movement. Thus, photothermal imaging of lipid rafts with stoichiometrically functionalized SBD-nanoparticles is a promising route for the quantitative analysis of the dynamics of lipid rafts on live cells.

3. Conclusion

Lipid rafts are increasingly regarded as membrane structures having an important impact in major cellular functions, e.g., cell signaling, internalization of extracellular molecules and entities. Moreover, it is now clear that dysfunction of lipid rafts might influence the progression of diseases such as various cancers, HIV infection and Alzheimer's disease. Although numerous studies report improvements in the characterization of the structure, constitution and dynamics of lipid rafts on the cell membrane, there is still an unmet need to target lipid rafts without changing or influencing their overall integrity by avoiding chemical reactions or genetic mutations of their lipid components. In this study, we developed a monofunctionalized SBD-nanoparticle as the first non-membrane protein-based nanoparticle targeting agent for lipid raft imaging on live cells. SBD is a unique sphingolipid biomarker, and its inclusion into the Mix-matrix self-assembled monolayer enabled the purification of stoichiometrically SBD-functionalized gold nanoparticles by ion-exchange chromatography. This approach increases the options, hitherto restricted to affinity chromatography, for the preparation of stoichiometrically-functionalized nanoparticles; thus ion-exchange chromatography selectively removed non-functionalized, and hence non-charged, Mix-matrix capped gold nanoparticles and allowed the identification and isolation of nanoparticles bearing just one SBD peptide. Interestingly, this method is potentially applicable for the stoichiometric functionalization of nanoparticles with a range of other charged biomolecules. The monofunctionalized nanoparticles showed long-term high stability against major

aggregation factors common in biological media and specific binding to sphingolipid-enriched microdomains on live cells. The long-term biocompatibility of the SBD-nanoparticles also enabled their visualization by photothermal imaging of membrane domain dynamics with the clustering and mobility of clusters of SBD-nanoparticles over relatively long distances, e.g., a few micrometers, over long times. Therefore, the SBD-nanoparticles show important potential as non-membrane protein-based lipid raft nanoparticle targeting agents to improve our understanding of the biological function of lipid rafts. The ability demonstrated here to direct nanoparticles to lipid rafts through their functionalization with the SBD peptide also opens the possibility of directing nanoparticles carrying additional functions to lipid rafts. Together with the exploitation of the physical properties of the nanoparticle itself in photothermal imaging and localized heating of the nanoparticle's immediate environment through the photothermal effect, the SBD-nanoparticles provide the means to manipulate cell function at the level of lipid rafts for experimental, and in due course therapeutic purposes. Eventually, this knowledge brings hope for the development of novel diagnostics and therapeutics by using specific lipid markers as an alternative to the limitations of membrane proteins as targets.[12]

4. Experimental Section

Materials and chemicals: Peptides H-CVVVT-ol and H-CVVVT-EG$_4$-SBD were purchased from Peptide and Protein Research (PPR Ltd., Hampshire, UK). HS-EC$_{11}$-EG$_4$ ligand was purchased from Prochimia (ProChimia Surfaces Sp. z o.o., Sopot, Poland). Gold nanoparticles of 8.2 nm diameter stabilized in citrate buffer were purchased from British Biocell (BBInternational Ltd., UK). Dimethylsulfoxide (DMSO), methanol, bovine serum albumin (BSA) (cat no. 9048-46-8), TRIS buffer pH8 and Tween 20 were purchased from Sigma-Aldrich Ltd. Nano-sep filters 10 kDa cut off were from PALL (PALL Corp., Portsmouth, Hants, UK). Sephadex G25 Fine and diethylaminoethyl (DEAE) Sepharose Fast Flow (GE Healthcare) were obtained from SciMed (Asia) Pte Ltd (Singapore). UV spectra were

acquired using the Spectra Max Plus spectrophotometer (Molecular Devices, Wokingham, UK) and 384 wells plates from Corning (Lowell, US).

Preparation of SBD functionalized Mix-matrix capped gold nanoparticles: The coating of gold nanoparticles with mixtures of peptidol and alkane thiol ethylene glycol ligands was done following the method previously published.[22] Briefly, in autoclaved plastic micro-tubes or glass containers, 9 volumes of citrate coated gold nanoparticles were added to 1 volume of 2 mM capping ligands mixture at room temperature. The 2 mM ligand capping mixtures used were of ratio 30:70 (mole/mole) of HS-EC$_{11}$-EG$_4$ to H-CVVVT-ol prepared by dilution of fresh stock solutions of ligands at 10 mM in water:DMSO 75:25 (v/v). When functionalized nanoparticles were prepared, an additional volume corresponding to the desired percentage of 2 mM stock solution of the H-CVVVT-EG$_4$-SBD prepared in water:DMSO 75:25 (v/v) was introduced in the ligand mixture (100% in Figure 3 corresponding to 1 volume of the capping peptidol ligand). After 1 min, the solution was mixed with 1 volume of PBS 10X (81 mM Na$_2$HPO$_4$, 12 mM KH$_2$PO$_4$, 1.4 M NaCl, and 27 mM KCl, pH 7.4) and 0.005 volume of a 1% (v/v) solution of Tween 20 in milliQ H$_2$O and left on a rotating wheel overnight at room temperature.

The excess of ligands was removed by size-exclusion chromatography (SEC) using Sephadex G25 columns with a mobile phase of 100 mM NaCl and 0.002% (v/v) Tween-20. The nanoparticle solutions were first concentrated by filtration with Nanosep 10kDa filters to obtain a volume of solution equivalent to 5-10% of the total volume of resin in the SEC columns. Depending on purification volume, a standard 1.5 cm x 14 cm column (Econo-Pac, Bio-Rad Laboratories (Singapore) Pte Ltd.) or XK 26 / XK 50 column (GE Healthcare, supplied by SciMed (Asia) Pte Ltd.) were used. Nanoparticles were then exchanged into 20 mM TRIS buffer pH8 by filtration with Nanosep 10 kDa filters, washing the nanoparticles three times with TRIS buffer by centrifugation for 3 min at 12,000 rcf.

Purification of SBD functionalized Mix-matrix capped gold nanoparticles by ion-exchange chromatography: To a column containing diethylaminoethyl (DEAE) Sepharose Fast Flow resin equilibrated in 20 mM TRIS buffer pH8, a volume of functionalized gold nanoparticles corresponding to 10% of the total volume of the resin was added. Non-functionalized nanoparticles were eluted from the column with 20 mM TRIS, pH8. After complete removal of all non-binding nanoparticles, functionalized nanoparticles were released from the resin with a 100 mM NaCl and 20mM TRIS, pH8. The solvent of each sample was then exchanged by filtration with Nanosep 10kDa filters and washings with PBS buffer pH7.4.

Photothermal Imaging Set-up: All images were taken using our homebuilt photothermal confocal microscope according to the design of Lounis and coworkers.[34,35] The excitation laser (532 nm; diode, Ventus Laser Quantum, Germany) was modulated at a frequency of 459.5 kHz using an acousto-optical modulator (Isomet, UK). This heating beam was then 'cleaned' using a spatial filter, to give the beam a Gaussian profile, and remove ellipticity generated by the modulation. The excitation beam was then overlaid with a non-resonant probe laser (633 nm; JDSU) via a cold mirror (ThorLabs, Germany). The superimposed beams were guided onto the sample via an oil immersion objective (Zeiss Plan-Apochromat 63x, numerical aperture (NA) 1.4). The sample was held in a fixed position upon a piezo scanning stage (MCL 502385, MadCity Labs, WI, USA), which allowed movement of the sample in 3 dimensions (x, y, and z) over the fixed laser spot. The scanning was controlled by piezo stage driver (MCL NanoDrive 85, Mad City Labs, WI, USA) under the control of the Nanonis RC4 module and Nanonis program (Specs Zurich, Germany). All scans were of a 70 x 70 μm area with a pixel size of approximately 100 nm. The light leaving the sample was collected by a second oil objective (Zeiss Neofluar 40x, NA 1.3). This light was passed through a high pass filter to remove light arising from the excitation laser, and was focused upon one photodiode of a balanced photodiode (Model 2107 10 MHz adjustable photoreceiver, New Focus, USA). A lock-in amplifier (DSP 7260, Signal Recovery, IL, USA)

was used to identify the scattered component of the probe beam that corresponds to the modulation frequency or 'beat-note', i.e., 459.5 kHz. The signal was acquired by the Nanonis SC4 Acquisition Module. The signal was averaged over a period of 1 ms for most imaging applications and a pixel value was generated. The values correspond to the scan path, and hence an image of the photothermal signal at each position was generated. The images were finally saved in an .sxm format. Raw data files were converted to .txt files using the freeware program Gwyddion for analysis.

Image analysis: Identification of peaks corresponding to nanoparticle labelled sphingolipid microdomains was achieved by thresholding the images using ImageJ. Images of labelled cells were thresholded with a value equal to that of the peak mitochondrial signals observed in unlabeled cells (250 mV). The image was then converted to a binary image and regions of interest (ROI) for each detected peak in the image generated. This selection was then applied to the original unmodified image, and the maximum intensity of each ROI measured. To deduce the approximate number of nanoparticles contributing to the peak, the maximum measured photothermal signal values were divided by the value for a single 8.2 nm gold nanoparticle.

Incubation of Neuroblastoma cells with SBD-NPs for photothermal imaging: Human SK-N-AS neuroblastoma cells (a gift from Anne Hermann, University of Liverpool) were pre-incubated with 10 mg/mL BSA (Sigma Aldrich, cat no. 9048-46-8) in a buffer that was nine parts PBS pH 7.4 (8.1 mM Na_2HPO_4, 1.2 mM KH_2PO_4, 140 mM NaCl, and 2.7 mM KCl) to one part Krebs Ringer (10 mM Hepes pH 7.4, 140 mM NaCl, 5 mM KCl, 2 mM $CaCl_2$, 2 mM $MgCl_2$, and 11 mM glucose) for fifteen minutes. Cells were then washed with PBS and incubated with 125 nM SBD-NPs in 10 mg/mL BSA PBS:Ringer for 30 minutes, after which the cells were washed three times with 10 mg/mL BSA PBS: Ringer buffer and mounted in Krebs Ringer buffer for photothermal imaging.

[1]   K. Simons, E. Ikonen, *Nature* **1997**, *387*, 569.

[2]   U. Coskun, K. Simons, *FEBS Lett.* **2010**, *584*, 1685.

[3]   K. Simons, M. J. Gerl, *Nat. Rev. Mol. Cell Biol.* **2010**, *11*, 688.

[4]   A. El-Sayed, H. Harashima, *Mol. Ther.* **2013**, *21*, 1118.

[5]   S. N. Stahley, M. Saito, V. Faundez, M. Koval, A. L. Mattheyses, A. P. Kowalczyk, *PLoS One* **2014**, *9*, e87809.

[6]   D. C. Anderson, *Drug Dev. Res.* **2013**, *74*, 92.

[7]   B. B. Diaz-Rohrer, K. R. Levental, K. Simons, I. Levental, *Proc. Natl. Acad. Sci. U. S. A.* **2014**, *111*, 8500.

[8]   A. Pralle, P. Keller, E. L. Florin, K. Simons, J. K. Hörber, *J. Cell Biol.* **2000**, *148*, 997.

[9]   F. Pinaud, X. Michalet, G. Iyer, E. Margeat, H.-P. Moore, S. Weiss, *Traffic* **2009**, *10*, 691.

[10]   L. Zhong, G. Zeng, X. Lu, R. C. Wang, G. Gong, L. Yan, D. Huang, Z. W. Chen, *PLoS One* **2009**, *4*, e5945.

[11]   N. Fabelo, V. Martín, R. Marín, D. Moreno, I. Ferrer, M. Díaz, *Neurobiol. Aging* **2014**, *35*, 1801.

[12]   V. Lladó, D. J. López, M. Ibarguren, M. Alonso, J. B. Soriano, P. V Escribá, X. Busquets, *Biochim. Biophys. Acta* **2014**, *1838*, 1619.

[13]   J. C. Chang, S. J. Rosenthal, *ACS Chem. Neurosci.* **2012**, *3*, 737.

[14]   M. Skočaj, N. Resnik, M. Grundner, K. Ota, N. Rojko, V. Hodnik, G. Anderluh, A. Sobota, P. Maček, P. Veranič, K. Sepčić, *PLoS One* **2014**, *9*, e92783.

[15]   M. Skočaj, B. Bakrač, I. Križaj, P. Maček, G. Anderluh, K. Sepčić, *Curr. Med. Chem.* **2013**, *20*, 491.

[16]   O. Beutel, J. Nikolaus, O. Birkholz, C. You, T. Schmidt, A. Herrmann, J. Piehler, *Angew. Chem. Int. Ed. Engl.* **2014**, *53*, 1311.

[17]   R. Mahfoud, N. Garmy, M. Maresca, N. Yahi, A. Puigserver, J. Fantini, *J. Biol. Chem.* **2002**, *277*, 11292.

[18]   S. Hebbar, E. Lee, M. Manna, S. Steinert, G. S. Kumar, M. Wenk, T. Wohland, R. Kraut, *J. Lipid Res.* **2008**, *49*, 1077.

[19]   S. Steinert, E. Lee, G. Tresset, D. Zhang, R. Hortsch, R. Wetzel, S. Hebbar, J. R. Sundram, S. Kesavapany, E. Boschke, R. Kraut, *PLoS One* **2008**, *3*, e2933.

[20]   J. Sankaran, M. Manna, L. Guo, R. Kraut, T. Wohland, *Biophys. J.* **2009**, *97*, 2630.

[21]   D. Zhang, M. Manna, T. Wohland, R. Kraut, *J. Cell Sci.* **2009**, *122*, 3715.

[22]   X. Chen, W. W. Qoutah, P. Free, J. Hobley, D. G. Fernig, D. Paramelle, *Aust. J. Chem.* **2012**, *65*, 266.

[23]   P. Free, D. Paramelle, M. Bosman, J. Hobley, D. G. Fernig, *Aust. J. Chem.* **2012**, *65*, 275.

[24]   L. Duchesne, D. Gentili, M. Comes-Franchini, D. G. Fernig, *Langmuir* **2008**, *24*, 13572.

[25]   R. Lévy, N. T. K. Thanh, R. C. Doty, I. Hussain, R. J. Nichols, D. J. Schiffrin, M. Brust, D. G. Fernig, *J. Am. Chem. Soc.* **2004**, *126*, 10076.

[26]   R. Lévy, Z. Wang, L. Duchesne, R. C. Doty, A. I. Cooper, M. Brust, D. G. Fernig, *ChemBioChem* **2006**, *7*, 592.

[27]   T. Lauterbach, M. Manna, M. Ruhnow, Y. Wisantoso, Y. Wang, A. Matysik, K. Oglecka, Y. Mu, S. Geifman-Shochat, T. Wohland, R. Kraut, K. Oglęcka, *PLoS One* **2012**, *7*, e51222.

[28]   S. A. Poulsen, A. A. Watson, D. P. Fairlie, D. J. Craik, *J. Struct. Biol.* **2000**, *130*, 142.

[29]   K. Bacia, D. Scherfeld, N. Kahya, P. Schwille, *Biophys. J.* **2004**, *87*, 1034.

[30]   P.-F. Lenne, L. Wawrezinieck, F. Conchonaud, O. Wurtz, A. Boned, X.-J. Guo, H. Rigneault, H.-T. He, D. Marguet, *EMBO J.* **2006**, *25*, 3245.

[31]   C. Leduc, S. Si, J. Gautier, M. Soto-Ribeiro, B. Wehrle-Haller, A. Gautreau, G. Giannone, L. Cognet, B. Lounis, *Nano Lett.* **2013**, *13*, 1489.

[32]   C. Eggeling, C. Ringemann, R. Medda, G. Schwarzmann, K. Sandhoff, S. Polyakova, V. N. Belov, B. Hein, C. von Middendorff, A. Schönle, S. W. Hell, *Nature* **2009**, *457*, 1159.

[33]   L. Duchesne, V. Octeau, R. N. Bearon, A. Beckett, I. A. Prior, B. Lounis, D. G. Fernig, *PLoS Biol.* **2012**, *10*, e1001361.

[34]   S. Berciaud, L. Cognet, G. A. Blab, B. Lounis, *Phys.Rev.Lett.* **2004**, *93*, 257402.

[35]   S. Berciaud, D. Lasne, G. Blab, L. Cognet, B. Lounis, *Phys. Rev. B* **2006**, *73*, 045424.

A

B

Alzheimer
β-amyloid ^{1}DAEFRHDSGYEVHHQ^{16}ELVFFAEDVG^{25}

H-CVVVT-EG$_4$-DAEFRHDSGYEVHHQ^{16}KLVFFAEDVG-OH

Coating Spacer   Sphingolipid-binding
peptide   domain peptide
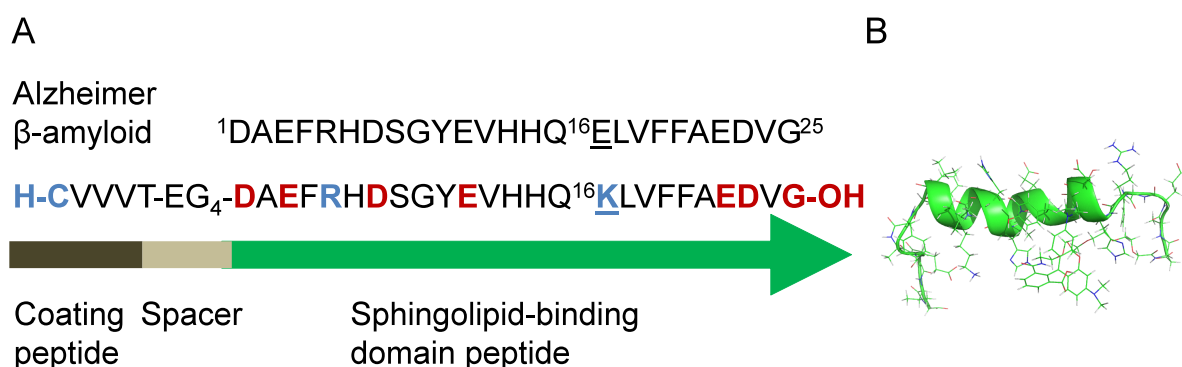
Figure 1. Structure of the SBD peptide. A) The Alzheimer β-amyloid peptide and the designed H-CVVVT-EG$_4$-SBD peptide ligand with a K16 mutation. Residues positively and negatively charged in solution at pH 8 are highlighted in blue and red, respectively. B) PDB structure of the peptide SBD K16. The N-terminus is on the left side of the structure.
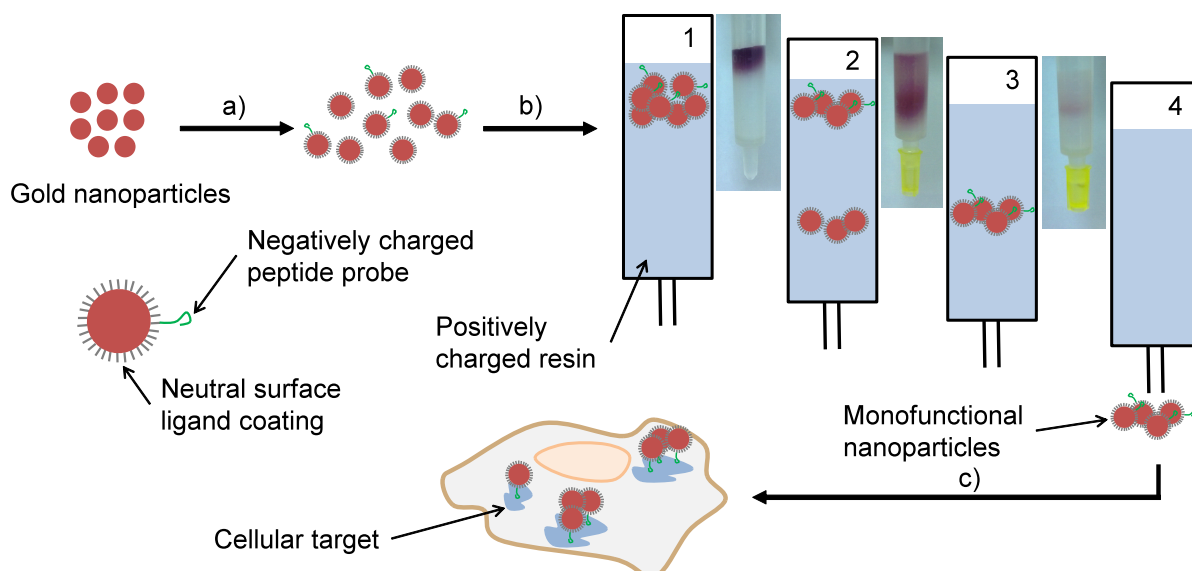
Figure 2. Preparation of stoichiometrically functionalized gold nanoparticles with a charged peptide biomarker. a) Coating and functionalization of gold nanoparticles in solution. b) Purification of stoichiometrically functionalized gold nanoparticles by ion-exchange chromatography; 1) deposition of nanoparticles mixture; 2) removal of non-functionalized nanoparticles; 3) elution and 4) collection of charged functionalized nanoparticles. c) *In vitro* test of stoichiometrically functionalized gold nanoparticles.
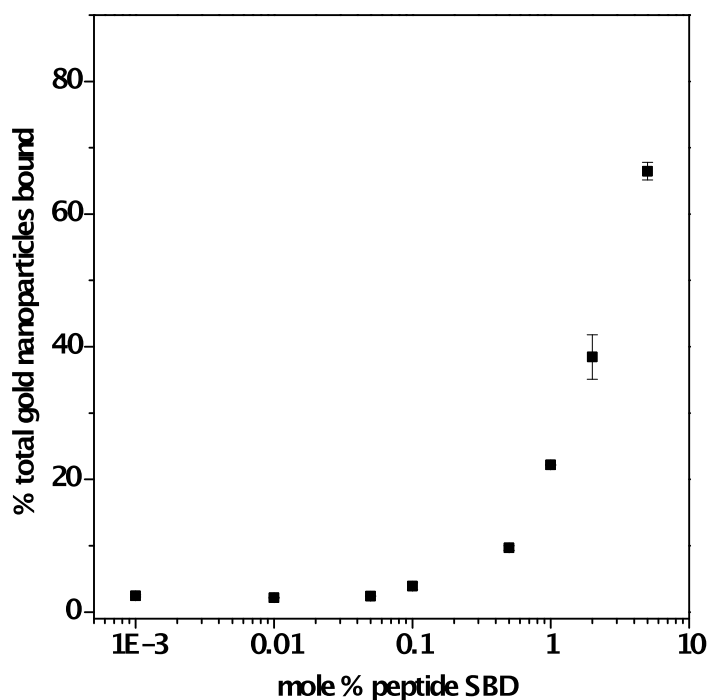
Figure 3. Titration of functionalization of 8.2 nm Mix-matrix capped gold nanoparticles with the sphingolipid-binding domain peptide ligand by ion-exchange chromatography.
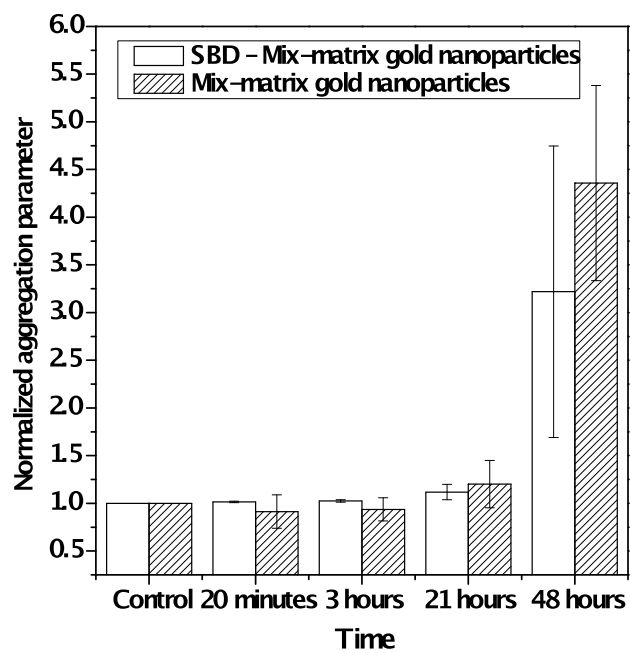
Figure 4. Ligand-exchange stability test of stoichiometrically functionalized SBD-nanoparticles. Normalized aggregation parameters after incubation in 0.5 M NaCl and 15 mM of DTT at pH 7.4 and room temperature.
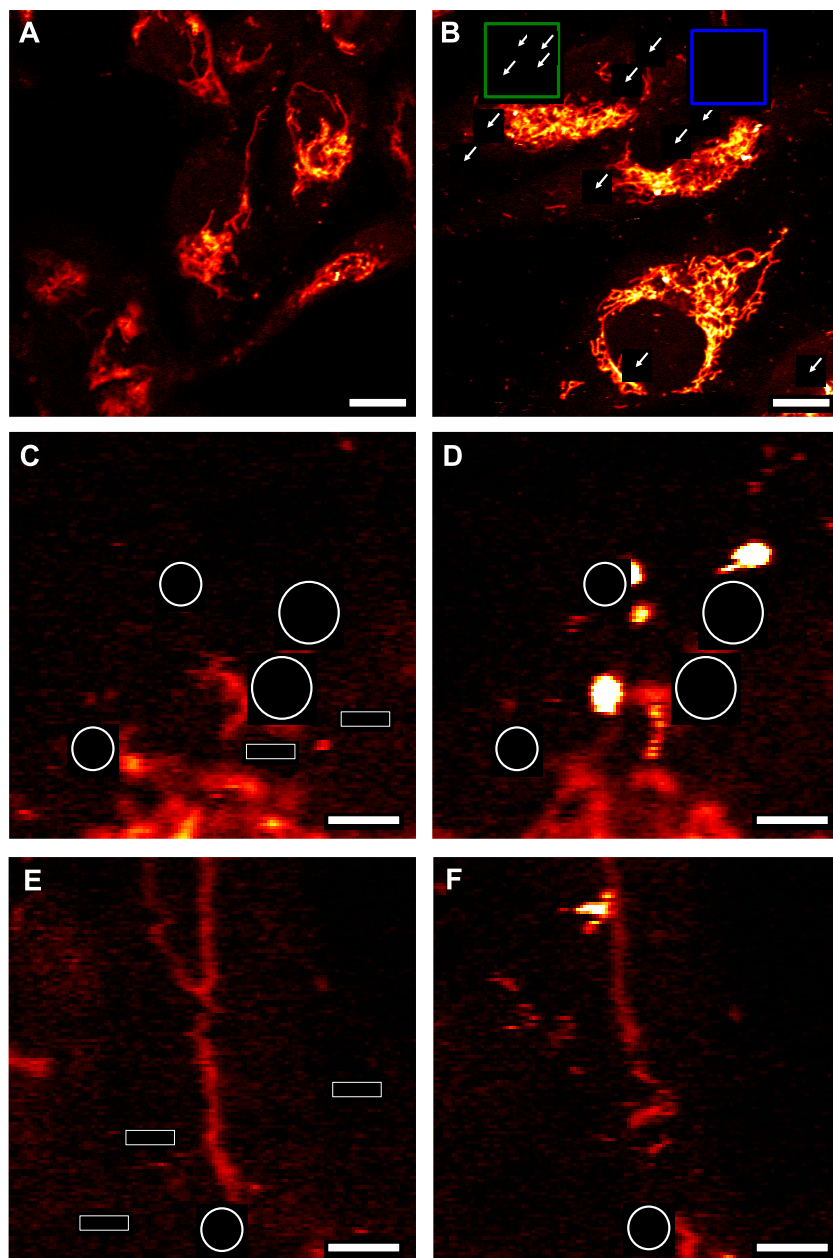
Figure 5. Photothermal imaging of monofunctionalized SBD nanoparticles labelled sphingolipids-enriched microdomains on SK-N-AS cell membranes. A) SK-N-AS cells incubated with 125 nM non-functionalized Mix-matrix nanoparticles. B) SK-N-AS cells labelled with 125 nM monofunctionalized SBD-nanoparticles. White arrows indicate photothermal peaks due to the presence of SBD-nanoparticles. C) Enlarged image corresponding to the green box in B). White circles correspond to the initial position of SBD-nanoparticles photothermal peaks, whereas white rectangles denote movement of single SBD-nanoparticles. D) Photothermal image of the same area as in C) after 10 min. White circles denote the positions of the intense peaks from C). E) Enlarged image from the blue box in B). White circles correspond to the initial position of SBD-nanoparticles photothermal peaks and white rectangles denote movement of single SBD-nanoparticles during the scan. F) Photothermal image of the same area as E) acquired 10 min later. The white circle denotes the original position of SBD-nanoparticles in E). Scale bars; A) and B) 10 μm and C) through F) 4 μm.

Table of content

Lipid raft targeting on live cells membrane is achieved with peptidol and thiolated alkane ethylene glycol ligand capped gold nanoparticles, stoichiometrically functionalized with a sphingolipid-binding domain peptide (SBD). Real-time photothermal microscopy reveals the dynamics of gold nanoparticles tagged lipid microdomains. The SBD-nanoparticles allow for non-membrane protein-based tracking of lipid rafts without prior chemical modification of the cells.
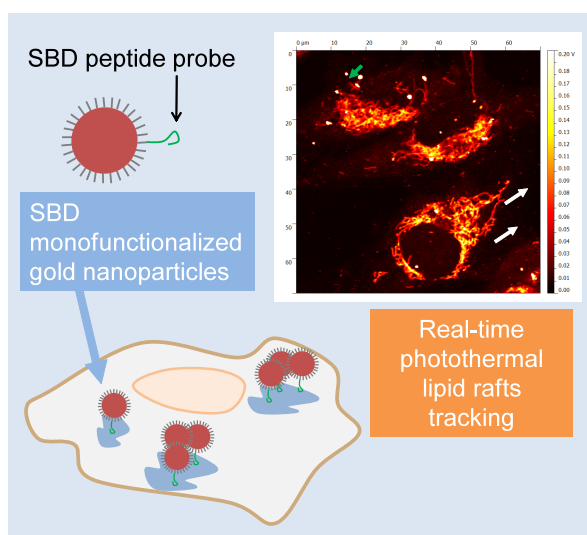
Keyword

Gold nanoparticles; monofunctionalization; lipid rafts; targeting agent; photothermal imaging

D. Paramelle,* D. Nieves, B. Brun, R. S. Kraut, and D. G. Fernig

Title

Targeting cell membrane lipid rafts by stoichiometric functionalization of gold nanoparticles with a sphingolipid-binding domain peptide
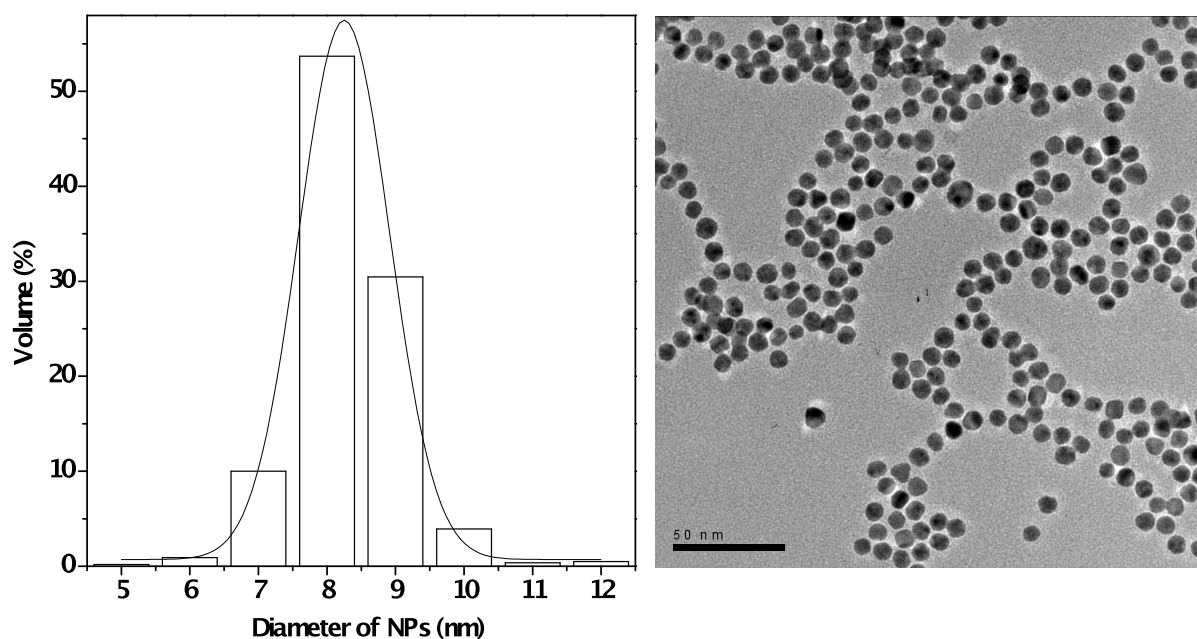
Supporting Information

Targeting cell membrane lipid rafts by stoichiometric functionalization of gold nanoparticles with a sphingolipid-binding domain peptide

David Paramelle,[*] Daniel Nieves, Benjamin Brun, Rachel S. Kraut, and David G. Fernig

Figure S1. Sizing of citrate coated spherical gold nanoparticles by high-resolution electronic microscopy. The average diameter is 8.2 ± 0.78 nm for 663 counts.
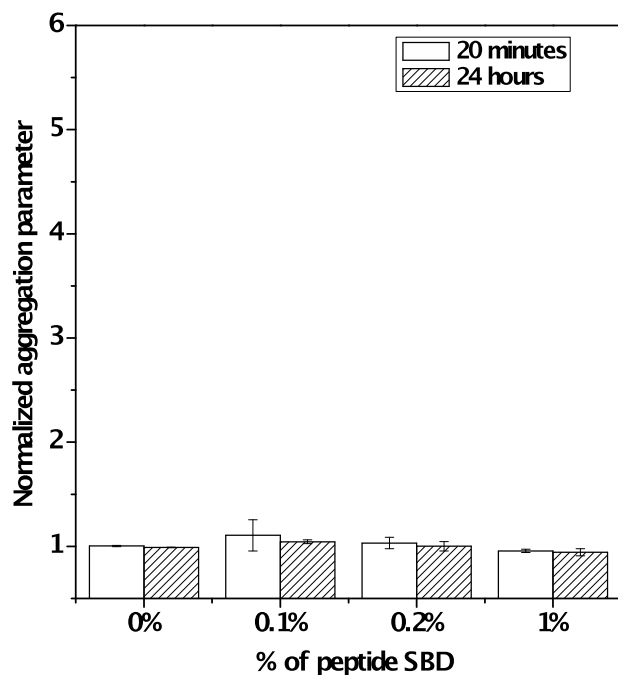
Figure S2. Electrolyte-induced aggregation test with 1 M of NaCl solution. Samples of gold nanoparticles capped with Mix-matrix prepared with 0, 0.1, 0.2 and 1% of H-CVVVT-EG$_4$-SBD peptide ligand were evaluated. A value of normalized aggregation parameter of 1 corresponds to a stable colloidal solution. Here, all samples were stable after two days.
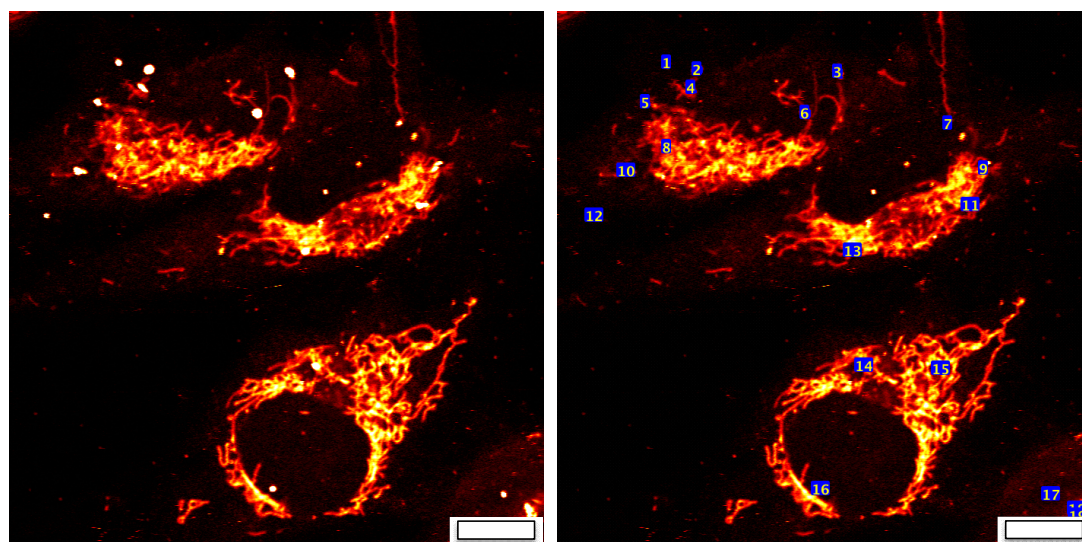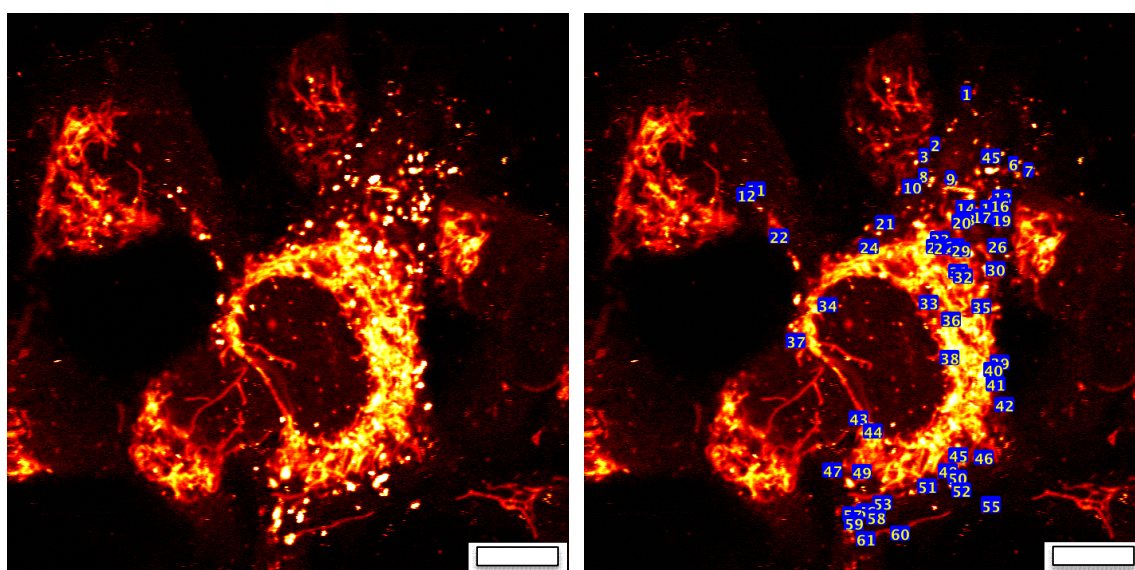

Figure S3. Photothermal Image of SK-N-AS cells labeled with 125 nM SBD-NPs (right). Detected sphingolipid microdomains from thresholding analysis are denoted by number in blue (left). Scale bar is 10 μm.
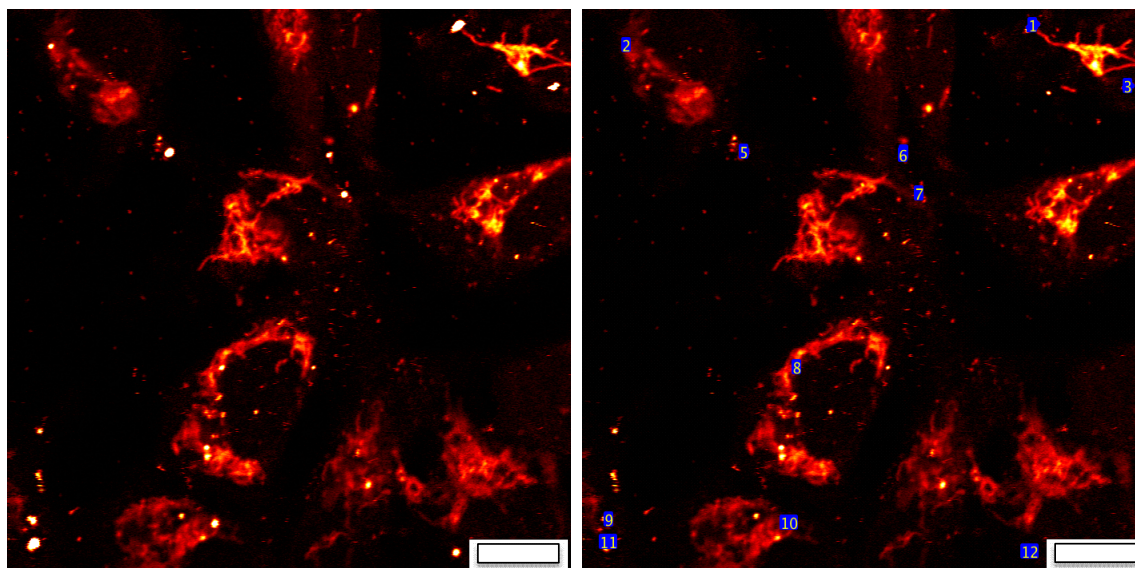
Figure S4. Photothermal Image of SK-N-AS cells labelled with 125 nM SBD-NPs (right). Detected sphingolipid microdomains from thresholding analysis are denoted by number in blue (left). Scale bar is 10 μm.

Figure S5. Photothermal Image of SK-N-AS cells labeled with 125 nM SBD-NPs. Detected sphingolipid microdomains from thresholding analysis are denoted by number in blue (left). Scale bar is 10 μm.

Number of sphingolipids per photothermal peak was calculated by dividing the maximum intensity of the photothermal peak by the intensity for a single nanoparticle in this optical

system, assuming a 1:1 stoichiometry of sphingolipid to bound nanoparticle. The number is then rounded down to the nearest whole nanoparticle.

Table S1. No. Particles per photothermal peak from Figure S3.

Peak	No. Particles	Peak	No. Particles
1	85	11*	66
2	77	12	23
3	148	13*	49
4*	49	14*	63
5	63	15*	16
6	119	16	73
7	20	17	46
8	32	18*	28
9*	23	19*	18
10*	59		

* denotes where the mitochondrial background may contribute to the measured and thus calculated value. These peaks correspond to the dashed blue circles within Figure S3.

Table S2. No. Particles per photothermal peak from Figure S4.

Peak	No. Particles	Peak	No. Particles
1	126	8*	18
2*	21	9	24
3	73	10*	23
4	21	11	270
5	98	12	24

6	21
7*	53

* denotes where the mitochondrial background may contribute to the measured and thus calculated value. These peaks correspond to the dashed blue circles within Figure S4.

Table S3. No. Particles per photothermal peak from Figure S5.

Peak	No. Particles	Peak	No. Particles
1	20	32*	41
2	50	33*	22
3	62	34	19
4	23	35*	19
5	41	36*	36
6	16	37*	22
7	29	38*	21
8	45	39*	39
9	103	40*	37
10	27	41	37
11	24	42	23
12	27	43*	36
13*	30	44*	17
14*	26	45*	21
15*	29	46*	20
16*	35	47	3
17*	27	48*	26
18*	25	49*	19

19*	17	50	56
20*	27	51*	28
21	27	52*	22
22*	18	53*	10
23*	34	54*	17
24*	17	55	23
25*	33	56*	41
26	40	57*	20
27*	28	58*	50
28*	68	59*	21
29*	28	60	20
30*	42	61*	19
31*	43		